Nanoscale Horizons

ROYAL SOCIETY OF CHEMISTRY

COMMUNICATION

View Article Online
View Journal | View Issue

Cite this: *Nanoscale Horiz.*, 2023, **8**, 127

Received 7th October 2022,
Accepted 3rd November 2022

DOI: 10.1039/d2nh00472k

rsc.li/nanoscale-horizons

Microbatteries with twin-Swiss-rolls redefine performance limits in the sub-square millimeter range†

Yang Li,[abc] Minshen Zhu,*[ac] Dmitriy D. Karnaushenko,[a] Fei Li,[abc] Jiang Qu,[abc] Jinhui Wang,[abc] Panpan Zhang,[d] Lixiang Liu,[c] Rachappa Ravishankar,[c] Vineeth Kumar Bandari,[abc] Hongmei Tang,[abc] Zhe Qu,[abc] Feng Zhu,*[abce] Qunhong Weng*[cf] and Oliver G. Schmidt*[abcg]

To maintain the downscaling of microelectronic devices with footprints less than one square millimeter, next-generation microbatteries should occupy the same area and deliver adequate energy for running a new generation of multi-functional microautonomous systems. However, the current microbattery technology fails in accomplishing this task because the micrometer-sized electrodes are not compatible with on-chip integration protocols and technologies. To tackle this critical challenge, an on-chip Swiss-roll microelectrode architecture is employed that exploits the self-assembly of thin films into ultra-compact device architectures. A twin-Swiss-roll microelectrode on a chip occupies a footprint of 0.045 mm^2 and delivers an energy density up to 458 μW h cm^{-2}. After packaging, the footprint of a full cell increases to 0.11 mm^2 with a high energy density of 181 μW h cm^{-2}. The volumetric energy density excluding the chip thickness is 16.3 mW h cm^{-3}. These results open opportunities for deploying microbatteries as energy and power sources to drive smart dust microelectronics and microautonomous systems.

New concepts

A fundamental barrier against the take-off of smart dust capable of detecting everything from light to vibrations to temperature that aims to revolutionize the Internet of Things is the spatial and time limitations of the power supply by energy conversion devices. A tiny battery of the same size could address this challenge. However, the integration of batteries into smart dust devices is plagued by the large gap in size between microbatteries and smart dust, as well as by the lack of energy supply for microbatteries to drive electronic functions. In this work, we develop microscale Swiss rolls on a chip by the self-assembly of nanomembranes, which is known as the micro-origami technology. The footprint of the battery based on the micro-Swiss-roll electrodes enters the deep submillimeter range (<0.1 mm^2). Moreover, the micro-Swiss-roll electrode mimics the most successful way to create an energy-dense battery: winding electrode materials up. As such, the energy density is around 0.46 mW h cm^{-2}, comparable to batteries two orders of magnitude larger (>1 mm^2). The micro-origami technology is expected to provide a new platform to create energy-dense batteries less than one millimeter across.

Introduction

Microelectronic chips have already entered the sub-1 mm^2 size region and they need on-board electricity to drive their functions.[1–3] As the tiny footprint sets stringent requirements for on-chip process flows and materials choices, the power supply is often provided by easy-to-fabricate miniaturized energy harvesters like piezoelectric generators or solar cells.[4–6] Unfortunately, these harvesters are often plagued by discontinuous supply of electricity because the external energy sources (vibration or solar light) are either location- or time-dependent. Batteries, instead, can ensure a stable current supply as their energy storage ability does not depend on external conditions.[7–12] However, on-chip microbatteries urgently need to be downscaled to the same footprint as their microelectronic counterparts and they must be capable of delivering adequate energy to continuously drive the many functions demanded by ever more complex microautonomous systems.[13]

Engineering 2D active thin-film materials into three-dimensional (3D) structures is an effective way to enhance the energy storage ability of microbatteries while maintaining

[a] *Research Center for Materials, Architectures and Integration of Nanomembranes (MAIN), Chemnitz University of Technology, Chemnitz, 09126, Germany*
[b] *Material Systems for Nanoelectronics, Chemnitz University of Technology, Chemnitz, 09107, Germany*
[c] *Institute for Integrative Nanosciences, Leibniz IFW Dresden, Dresden, 01069, Germany*
[d] *State Key Laboratory of Materials Processing and Die & Mould Technology, School of Materials Science and Engineering, Huazhong University of Science and Technology, Wuhan, 430074, China*
[e] *State Key Laboratory of Polymer Physics and Chemistry, Changchun Institute of Applied Chemistry, Chinese Academy of Sciences, Changchun, 130022, China*
[f] *School of Materials Science and Engineering, Hunan University, Changsha, 110016, China*
[g] *School of Science, Dresden University of Technology, Dresden, 01069, Germany*

† Electronic supplementary information (ESI) available. See DOI: https://doi.org/10.1039/d2nh00472k

a small footprint.[14–19] 3D microbatteries often consist of interdigitated electrodes with a large aspect ratio of height to footprint in an attempt to maximize material loading of the electrode.[20–22] The energy density of such a 3D microbattery can reach up to 1 mW h cm^{-2}.[23] However, its footprint is larger than 9 mm^2 and very few prototypes with an area of less than 1 mm^2 have been reported. It is thus important to develop a novel technology to produce the 3D structure with a reduced footprint while keeping high electroactive materials loading. Alternatively, a micro-origami self-assembly process is able to transform a large-area thin film into a micrometer-sized Swiss-roll, which bypasses this technological difficulty.[24] The fabrication of the Swiss-rolls follows an on-chip processing route which is compatible with the manufacturing of microelectronic devices.[25]

Herein, a self-assembly process is demonstrated to create a high-performance microbattery using Swiss-roll microelectrodes. A pair of patterned thin films (Ti and Au) is wound up into a compact microstructure, in this way shrinking the footprint of the Swiss-roll microelectrode by ten times compared to that of the flat thin film, merely occupying a final area of 0.021 mm^2. The Swiss-roll microelectrodes are generated by depositing MnO_2 and Zn. The energy density of the Zn–MnO_2 microbattery with a footprint of less than 0.1 mm^2 attains 458 μW h cm^{-2}.

Results and discussion

Reshape a 2D flat layer into a 3D mesostructured Swiss-roll

A micro-origami technology is utilized to create Swiss-roll microelectrodes (Fig. 1a). Three layers (photoresist, Ti, and Au) are consecutively deposited and patterned on a chip surface. During deposition differential strain builds up between the Ti and Au layer (Ti/Au layer).[26] Upon releasing the strain by etching away the photoresist sacrificial layer the Ti/Au layer winds up automatically forming a Swiss roll. First of all, the diameter depends on the thickness of Ti/Au layer. As shown in Fig. S1 (ESI†), the diameter of the Swiss-roll electrode increases with the increasing thickness of the Ti/Au layer. Here we use 30 nm Ti and 30 nm Au for further development. Microscale holes are also patterned into the Ti and Au layers (Fig. 1b) to achieve better contact between the electrode materials and the electrolyte. As the holes in the Ti/Au layer greatly influence the built-in strain the finite element method (FEM) is used to investigate the effect of the perforated design on the final 3D Swiss-roll structure. The size of the single hole unit cell is defined as a square with the side length (L = 12 μm; Fig. 1c). The filling factor k is defined as the aspect ratio of the square-hole to the unit cell. The simulation result shows that the diameter of the first winding of the Swiss-roll increases as k becomes larger, which is confirmed by the scanning electron microscope

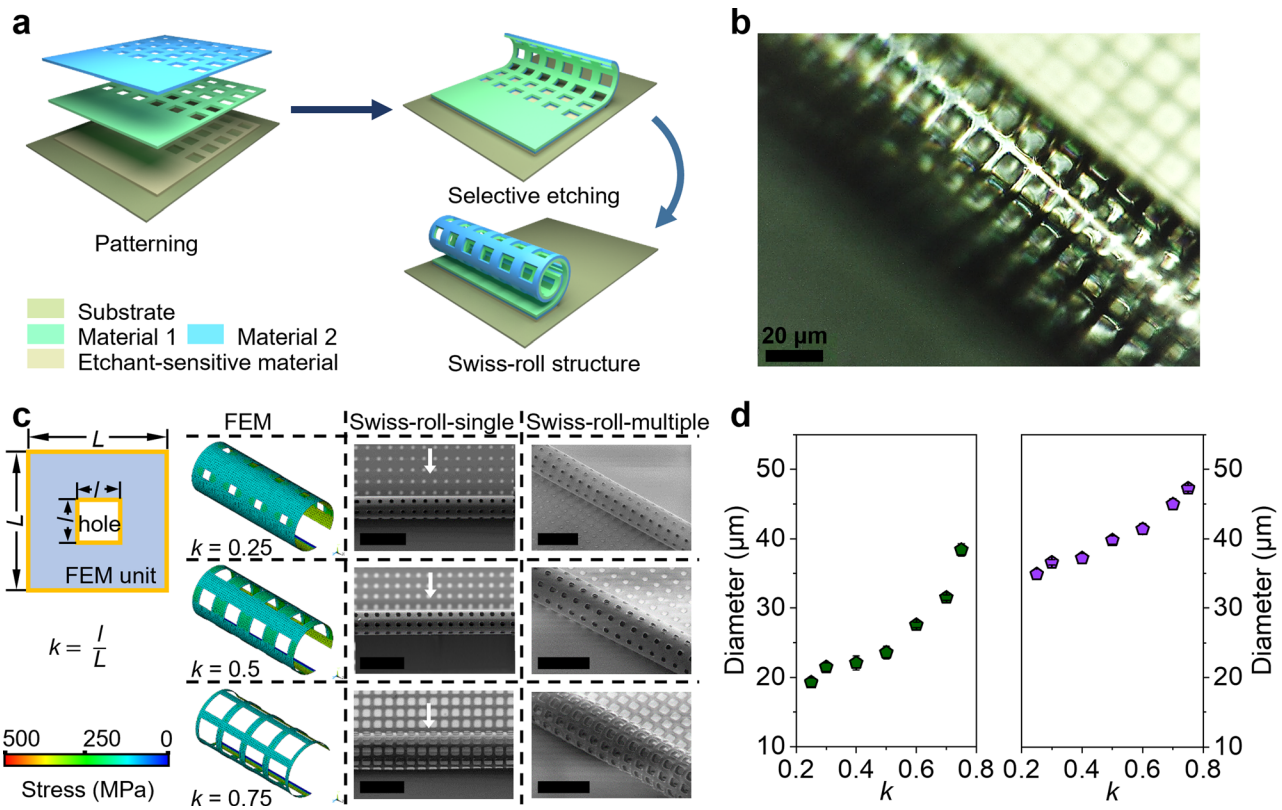

Fig. 1 Rational design of a 3D mesostructured Swiss-roll. (a) Schematic of the self-assembly process of a mesostructured Swiss-roll from a 2D layer precursor. (b) Optical microscope image of a mesostructured Swiss-roll (k = 0.75). (c) FEM simulations and SEM images of Swiss-rolls. Scale bars in SEM images: 50 μm. White arrows indicate rolling direction. (d) Diameter of Swiss-roll as a function of k value (left: Swiss-roll-single; right: Swiss-roll-multiple).

(SEM) images (Fig. 1c, Swiss-roll-single). Fig. 1d (left panel) provides details of the diameter change of the Swiss-roll as a function of k. As the first winding largely determines the diameter of the Swiss-roll an increase in diameter of Swiss-rolls after multiple windings (Fig. 1c, Swiss-roll-multiple) is observed. Since the diameter of the multiple-winding Swiss-roll is more than 10 μm larger than the first winding, one can infer that interlayer gaps do exist between neighboring windings (Fig. 1d, right panel). A large interlayer gap is beneficial for loading more electroactive materials into the microelectrodes to achieve a higher energy storage capacity. Fig. S2 (ESI†) shows the variation of the interlayer gap in the Swiss-roll as a function of k. As the interlayer gap reaches the maximum when k = 0.5, this k value is used as the design parameter in the following experiments.

The construction of Swiss-roll microelectrodes

To use the hollow Swiss-rolls as microelectrodes for an on-chip battery, the start edge for the micro-origami process is defined by anchoring the other three edges to the chip. Two perforated Ti/Au layers roll up against each other and form a twin tube architecture on a single chip (Fig. 2a). The footprint area of one perforated Swiss-roll is about 0.021 mm^2 (calculated from Fig. S3, ESI†). Then electroactive materials are deposited into the Ti/Au Swiss-roll current collectors to build a battery. Owing to the high stability in the air,[27–31] MnO_2 and Zn are used for deposition (Fig. 2a). The top (Fig. 2b) and side (Fig. 2c) views of the MnO_2 tubular structure show that MnO_2 is successfully deposited into the Swiss roll. A small amount of MnO_2 (0.8 μg) is loaded onto the Swiss-roll microelectrodes after 7 min deposition (the measurement of the weight is explained in the ESI†). The magnified SEM image in Fig. 2d shows the porous structure of the deposited MnO_2. Raman spectroscopy shows two peaks at 575 and 657 cm^{-1} (Fig. S4a, ESI†), which can be ascribed to the symmetric stretching vibration of the Mn–O bond in the MnO_6 octahedron and the Mn–O vibration along the chain of the MnO_2 framework, respectively.[32–34] The XRD diffraction peaks at 37.4°, 42.6°, 56.8°, and 64.7° further confirm the formation of MnO_2 (Fig. S4b, ESI†).[35] Zn metal corrosion in mild aqueous electrolyte is one of the main reasons for Zn battery with poor cycling performance.[36,37] In order to mitigate the corrosion induced capacity decay, excessive Zn (2.3 μg) was deposited into the Swiss-roll microelectrodes (Fig. 2e). Fig. 2f shows that the Swiss-roll is filled by Zn. The magnified SEM image (Fig. 2g) reveals the vertical growth of Zn nanosheets on the Au surface. XRD peaks of the deposited Zn are indexed to the hexagonal phase of Zn (JCPDS, No. 04-0831) (Fig. S4c, ESI†). Fig. S5 (ESI†) shows that the perforation reduces Young's modulus and stiffness of Swiss-roll electrodes, but the loading of Zn and MnO_2 strengthens the mechanical properties to allow for stable operation. The perforated Swiss-roll electrodes also show higher capacity than those without holes (Fig. S6a, ESI†) because the thickness of deposited materials (*e.g.*, MnO_2) in the perforated Swiss-roll electrode (Fig. S6b, ESI†) is much higher than in the unperforated Swiss-roll electrode (Fig. S6c, ESI†).

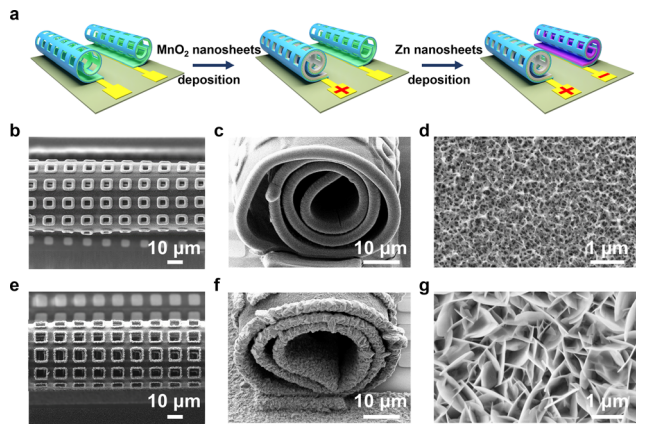

Fig. 2 Manufacture of mesostructured Swiss-roll microelectrodes. (a) Schematic of the Zn–MnO_2 Swiss-roll microbattery fabrication process. Top (b) and side view (c) SEM images of mesostructured Swiss-roll microcathode. (d) Magnified SEM image of the MnO_2 morphology. Top (e) and side (f) view of mesostructured Swiss-roll microanode. (g) Magnified SEM image of the Zn nanosheet morphology.

Electrochemical performance of microbattery

As the degradation of the Zn microanode is the main reason for battery failure, we first evaluated the Zn anode performance in the electrolyte. Fig. 3a displays the long-term galvanostatic cycling performance of a planar Zn anode (1 mm^2) at a current density of 200 μA cm^{-2}. The Zn/Zn symmetric cell shows stable voltage profiles for over 110 hours with a low overpotential of 34 mV confirming the excellent deposition/stripping reversibility of the Zn anode. Such low overpotential is attributed to the bulky $CF_3SO_3^-$ anions that decrease the number of water molecules surrounding Zn^{2+} cations, facilitating Zn^{2+} transportation and charge transfer.[38] Swiss-roll microelectrodes of MnO_2 and Zn are encapsulated by a SU8 box with a length of 600 μm and width of 190 μm (Fig. S7, ESI†). More specifically, the SU8 box is fabricated by a standard photolithography process (the details are described in the ESI†). One droplet of aqueous solution containing $Zn(CF_3SO_3)_2$ (3 mol L^{-1}) and $Mn(CF_3SO_3)_2$ (0.025 mol L^{-1}) is added to the SU8 box. To prevent evaporation of the electrolyte, a SU8 cover was placed onto the box. Fig. 3b shows the cyclic voltammetry (CV) curve of the Swiss-roll microbattery in the potential range of 0.8 to 1.8 V at a scan rate of 0.1 mV s^{-1}. The CV curve of the first cycle demonstrates two cathodic peaks located at 1.39 V and 1.21 V corresponding to the zinc ion insertion in MnO_2 and conversion reaction to MnOOH and Mn_2O_3, respectively.[39,40] During the anodic scan, two peaks located at around 1.62 and 1.68 V are observed, which are attributed to the extraction of protons and zinc ions from cathode, respectively.[41,42] In the following cycles, the cathodic peak at 1.39 V shifts to 1.42 V. A strong anodic peak at around 1.65 V emerges during the anodic sweep. Fig. 3c shows the galvanostatic charge/discharge (GCD) curves of the Swiss-roll microbattery after a conditioning cycle at a current density of 200 μA cm^{-2} (footprint of one Swiss-roll microelectrode: 0.021 mm^2). One pair of charge/discharge

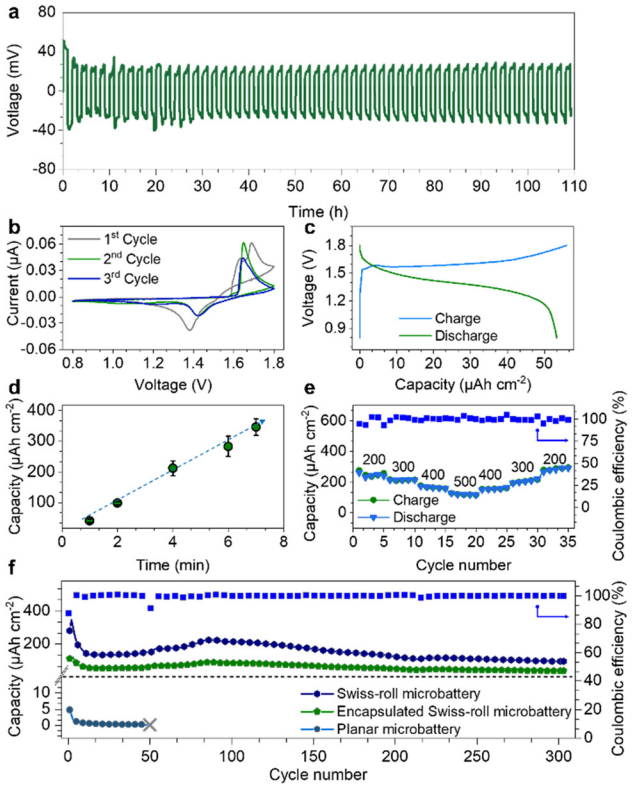

Fig. 3 Electrochemical performance of the Swiss-roll microbattery. (a) Galvanostatic cycling of Zn/Zn planar symmetrical cell at a current density of 200 μA cm^{-2}. (b) CV curve of the Swiss-roll microbattery collected at a scan rate of 0.1 mV s^{-1}. (c) GCD curves at a current density of 200 μA cm^{-2} (1 min MnO_2 deposition). (d) Effect of the MnO_2 deposition time on the areal capacity of microbatteries. (e) Rate performance of microbattery. (f) Cycling performance of Swiss-roll microbattery, encapsulated Swiss-roll microbattery, and planar microbattery at a current density of 500 μA cm^{-2}.

plateaus are observed at 1.65 V and 1.42 V, consistent with the CV curves. Fig. 3d indicates that the energy storage performance of the Swiss-roll microbattery is remarkably promoted by simply increasing the deposition time of MnO_2. The footprint capacity increases from 41 to 345 μA h cm^{-2} as the deposition time increases from 1 to 7 min (Fig. 3d). The gravimetric capacity and energy density of the MnO_2 Swiss-roll microelectrode are 194 mA h g^{-1} and 257 mW h g^{-1}, respectively, which are comparable to other MnO_2 based Zn ion batteries (Table S1, ESI†). The Swiss-roll microelectrode delivers a high footprint capacity of 130 μA h cm^{-2} at a current density of 500 μA cm^{-2} (Fig. 3e). The footprint capacity recovers to 300 μA h cm^{-2} when the current density is reduced to 200 μA cm^{-2}. Although the initial coulombic efficiency is less than 100% (90%) due to the structural change of MnO_2,[43] a reversible footprint capacity of 115 μA h cm^{-2} at the current of 500 μA cm^{-2} is attainable over 147 cycles with the coulombic efficiency of around 100% (Fig. S8, ESI†). Moreover, the cycling performance of the Swiss-roll microbattery is improved to 300 cycles with a reversible footprint capacity of 96 μA h cm^{-2} and a coulombic efficiency of around 99% (Fig. 3f) by increasing the Zn thickness to about 1 μm (Fig. S9, ESI†). As a higher thickness means a lower utilization rate of Zn anode, it is still necessary to improve the Zn reversibility at a high utilization rate. By contrast, planar electrodes with the same footprint area as the Swiss-roll microbattery show a low capacity of only 4 μA h cm^{-2} and short cycle life of less than 50 cycles (Fig. 3f). The poor performance of the planar electrodes is attributed to the delamination of MnO_2 from the current collector (Fig. S10, ESI†). In addition, the lifetime capacity of the Swiss-roll microelectrodes is 19.3 μA h (26 μW h) able to power a low-power (16 nW) temperature sensing microsystem with data processing capability for about two month,[44] demonstrating the practicability for the target application scenarios.

Fig. 4a compares the areal energy density of various microbatteries.[23,45–51] Microbatteries have two common architectures: layered thin films and interdigitated electrode strips on the surface.[45–47] Despite the high attainable energy density, they are larger than 1 mm^2 because of difficulties in shrinking the size, such as maintaining the structural integrity with a small footprint and accuracy of layering down tiny films. With a small footprint area, the cycling performance is often compromised (less than 50 cycles) because the instability issues of materials and electrode structure are amplified at a small scale.[45,46] For the first time, the electrode footprint (0.045 mm^2) enters an unexplored regime of less than 0.1 mm^2. Based on the electrode footprint, the energy density is 458 μW h cm^{-2}. After a simple package by a SU8 box on a chip (Fig. S7, ESI†), the footprint of a full cell is slightly larger than 0.1 mm^2 (0.11 mm^2). The capacity and energy density of the on-chip packaged Swiss-roll micobattery are 136 μA h cm^{-2} and 181 μW h cm^{-2}, respectively. The volumetric capacity and energy density excluding the chip thickness are 12.2 mA h cm^{-3} and

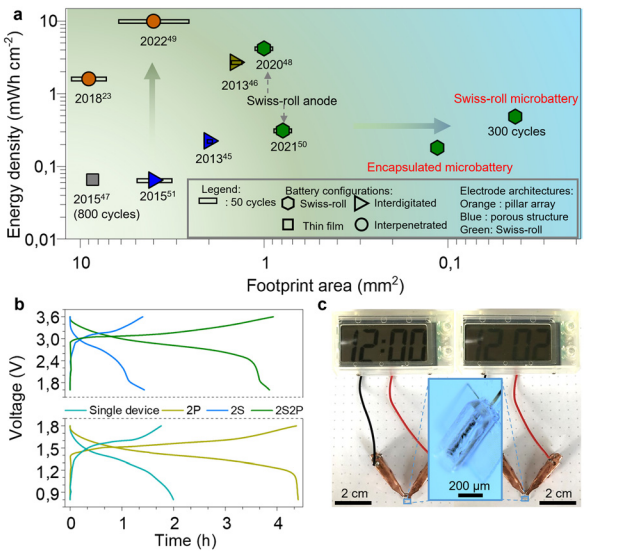

Fig. 4 Comparison of Swiss-roll microbattery performance. (a) Comparison of areal energy density, footprint area, and cycling performance of Swiss-roll microbatteries with previously reported ones. (b) GCD curves of microbatteries connected in series and parallel. (c) Digital photographs of Swiss-roll microbattery powering a digital watch for two min (inset is the encapsulated Swiss-roll microbattery).

16.3 mW h cm^{-3}, respectively. With the comparable energy density, the Swiss-roll microbattery is about one order of magnitude less than microbatteries with other architectures.[45,47,51] More importantly, the cycling stability is among the best of microbatteries. Swiss-roll microelectrode also show the potential to achieve a higher energy density by using high-capacity materials (*e.g.*, silicon, germanium).[48,50]

The microbattery can be connected in series and in parallel. The operation voltage doubles when two microbatteries are connected in series (Fig. 4b, upper panel). The charge/discharge time of two microbatteries connected in parallel (Fig. 4b, bottom panel) is twice that of the single one indicating twice capacity. Moreover, four microbatteries are assembled into a hybrid configuration, where two microbatteries are connected in series and then the series-connected microbatteries are connected in parallel (Fig. 4b, upper panel). This hybrid configuration attains a large capacity and high operational voltage. To demonstrate the feasibility for practical applications, the encapsulated microbattery is used as the power supply for electronic devices. As shown in Fig. 4c, the microbattery can power a digital watch with a screen for 2 min, implying that the Swiss-roll microbattery hold great promise in applications of integrated electronic devices.

Conclusions

In summary, a new strategy is presented to construct a microbattery with a footprint smaller than 0.1 mm^2. The self-assembly process of thin films driven by inherent built-in strain forms a Swiss-roll structure that mimics the most rational electrode design for bulk batteries. As a result, the loading of MnO_2 onto and into a microelectrode with a minimal footprint (0.021 mm^2) can be substantially increased for achieving a high capacity of up to 345 μA h cm^{-2}. Paired with a Zn Swiss-roll microanode, twin Swiss-roll electrodes occupy a small footprint of 0.045 mm^2 and deliver an energy density of 458 μW h cm^{-2}. Meanwhile, the on-chip packaged Swiss-roll micobattery with a footprint area of 0.11 mm^2 achieves a high capacity of up to 136 μA h cm^{-2} and an energy density of 181 μW h cm^{-2}. Furthermore, the on-chip fabrication procedure allows to build battery arrays in parallel in a single manufacturing run encouraging further development towards a new generation of microbatteries for autonomous microelectronic systems.

Author contributions

Yang Li, Minshen Zhu, Feng Zhu, Qunhong Weng, and Oliver G. Schmidt conceived the idea. Yang Li, Minshen Zhu, Feng Zhu, and Qunhong Weng designed experiments. Yang Li performed the experiment. Dmitriy D. Karnaushenko performed the FEM simulation. Lixiang Liu and Jiang Qu carried out XRD experiment. Yang Li, Jinhui Wang, and Vineeth Kumar Bandari contributed on the fabrication of microbattery. Yang Li, Panpan Zhang, and Zhe Qu contributed on the characterizations. Rachappa Ravishankar carried out AFM measurement. Fei Li and Hongmei Tang participated in analysis of the data. Yang Li, Minshen Zhu, Feng Zhu, Qunhong Weng, and Oliver G. Schmidt analyzed the results and wrote the manuscript with inputs from all authors.

Conflicts of interest

There are no conflicts to declare.

References

1 N. Ilyas, J. Wang, C. Li, D. Li, H. Fu, D. Gu, X. Jiang, F. Liu, Y. Jiang and W. Li, *Adv. Funct. Mater.*, 2021, **32**, 2110976.
2 K. Zhu, C. Wen, A. A. Aljarb, F. Xue, X. Xu, V. Tung, X. Zhang, H. N. Alshareef and M. Lanza, *Nat. Electron.*, 2021, **4**, 775–785.
3 Y. Li, M. Zhu, V. K. Bandari, D. D. Karnaushenko, D. Karnaushenko, F. Zhu and O. G. Schmidt, *Adv. Energy Mater.*, 2022, **12**, 2103641.
4 X. G. Guo, Z. G. Xue and Y. H. Zhang, *NPG Asia Mater.*, 2019, **11**, 1–7.
5 D. Karnaushenko, T. Kong, V. K. Bandari, F. Zhu and O. G. Schmidt, *Adv. Mater.*, 2020, **32**, 1902994.
6 L. Liu and S. Choi, *Biosens. Bioelectron.*, 2021, **177**, 112970.
7 C. Y. Liu, E. I. Gillette, X. Y. Chen, A. J. Pearse, A. C. Kozen, M. A. Schroeder, K. E. Gregorczyk, S. B. Lee and G. W. Rubloff, *Nat. Nanotechnol.*, 2014, **9**, 1031–1039.
8 M. S. Zhu, Z. G. Wang, H. F. Li, Y. Xiong, Z. X. Liu, Z. J. Tang, Y. Huang, A. L. Rogach and C. Y. Zhi, *Energy Environ. Sci.*, 2018, **11**, 2414–2422.
9 J. J. Shi, S. L. Wang, X. Chen, Z. C. Chen, X. Y. Du, T. Ni, Q. Wang, L. M. Ruan, W. Zeng and Z. X. Huang, *Adv. Energy Mater.*, 2019, **9**, 1901957.
10 Z. Lin, B. Xiao, M. Huang, L. Yan, Z. Wang, Y. Huang, S. Shen, Q. Zhang, L. Gu and W. Zhong, *Adv. Energy Mater.*, 2022, **12**, 2200855.
11 S. Shen, Z. Hu, H. Zhang, K. Song, Z. Wang, Z. Lin, Q. Zhang, L. Gu and W. Zhong, *Angew. Chem., Int. Ed.*, 2022, **61**, 202206460.
12 Z. Wang, S. Shen, Z. Lin, W. Tao, Q. Zhang, F. Meng, L. Gu and W. Zhong, *Adv. Funct. Mater.*, 2022, **32**, 2112832.
13 J. X. Zhao, H. Y. Lu, X. X. Zhao, O. I. Malyi, J. H. Peng, C. H. Lu, X. F. Li, Y. Y. Zhang, Z. Y. Zeng, G. C. Xing and Y. X. Tang, *ACS Mater. Lett.*, 2020, **2**, 1041–1056.
14 S. H. Zheng, X. Y. Shi, P. Das, Z. S. Wu and X. H. Bao, *Adv. Mater.*, 2019, **31**, 1900583.
15 L. Zhou, W. W. Ning, C. Wu, D. Zhang, W. F. Wei, J. M. Ma, C. C. Li and L. B. Chen, *Adv. Mater. Technol.*, 2019, **4**, 1800402.
16 K. Miyamoto, T. Sasaki, T. Nishi, Y. Itou and K. Takechi, *iScience*, 2020, **23**, 101317.
17 Z. Y. Lyu, G. J. H. Lim, J. J. Koh, Y. Li, Y. W. Ma, J. Ding, J. L. Wang, Z. Hu, J. Wang, W. Chen and Y. F. Chen, *Joule*, 2021, **5**, 89–114.
18 M. S. Zhu and O. G. Schmidt, *Nature*, 2021, **589**, 195–197.

19 Z. Qu, M. Zhu, Y. Yin, Y. Huang, H. Tang, J. Ge, Y. Li, D. D. Karnaushenko, D. Karnaushenko and O. G. Schmidt, *Adv. Energy Mater.*, 2022, **12**, 2200714.
20 J. W. Deng, X. Y. Lu, L. X. Liu, L. Zhang and O. G. Schmidt, *Adv. Energy Mater.*, 2016, **6**, 1600797.
21 X. F. Wang, Y. Chen, O. G. Schmidt and C. L. Yan, *Chem. Soc. Rev.*, 2016, **45**, 1308–1330.
22 Y. Li, J. Qu, F. Li, Z. Qu, H. Tang, L. Liu, M. Zhu and O. G. Schmidt, *Nano Mater. Sci.*, 2021, **3**, 140–153.
23 J. I. Hur, L. C. Smith and B. Dunn, *Joule*, 2018, **2**, 1187–1201.
24 B. Bao, B. Rivkin, F. Akbar, D. D. Karnaushenko, V. K. Bandari, L. Teuerle, C. Becker, S. Baunack, D. Karnaushenko and O. G. Schmidt, *Adv. Mater.*, 2021, **33**, 2101272.
25 Y. Lee, V. K. Bandari, Z. Li, M. Medina-Sanchez, M. F. Maitz, D. Karnaushenko, M. V. Tsurkan, D. D. Karnaushenko and O. G. Schmidt, *Nat. Commun.*, 2021, **12**, 4967.
26 T. M. Li, V. K. Bandari, M. Hantusch, J. H. Xin, R. Kuhrt, R. Ravishankar, L. Q. Xu, J. D. Zhang, M. Knupfer, F. Zhu, D. H. Yan and O. G. Schmidt, *Nat. Commun.*, 2020, **11**, 3592.
27 P. H. Yang, C. Z. Feng, Y. P. Liu, T. Cheng, X. L. Yang, H. D. Liu, K. Liu and H. J. Fan, *Adv. Energy Mater.*, 2020, **10**, 2002898.
28 J. Cao, D. D. Zhang, Y. L. Yue, X. Wang, T. Pakornchote, T. Bovornratanaraks, X. Y. Zhang, Z. S. Wu and J. Q. Qin, *Nano Energy*, 2021, **84**, 105876.
29 G. J. Liang and C. Y. Zhi, *Nat. Nanotechnol.*, 2021, **16**, 854–855.
30 S. Wang, Z. S. Yuan, X. Zhang, S. S. Bi, Z. Zhou, J. L. Tian, Q. C. Zhang and Z. Q. Niu, *Angew. Chem., Int. Ed.*, 2021, **60**, 7056–7060.
31 M. S. Zhu, J. P. Hu, Q. Q. Lu, H. Y. Dong, D. D. Karnaushenko, C. Becker, D. Karnaushenko, Y. Li, H. M. Tang, Z. Qu, J. Ge and O. G. Schmidt, *Adv. Mater.*, 2021, **33**, 2007497.
32 C. Julien, M. Massot, R. Baddour-Hadjean, S. Franger, S. Bach and J. P. Pereira-Ramos, *Solid State Ionics*, 2003, **159**, 345–356.
33 C. M. Julien and M. Massot, *Mater. Sci. Eng., B*, 2003, **100**, 69–78.
34 C. M. Julien, M. Massot and C. Poinsignon, *Spectrochim. Acta, Part A*, 2004, **60**, 689–700.
35 Q. W. Tang, L. H. Jiang, J. Liu, S. L. Wang and G. Q. Sun, *ACS Catal.*, 2014, **4**, 457–463.
36 J. N. Hao, X. L. Li, X. H. Zeng, D. Li, J. F. Mao and Z. P. Guo, *Energy Environ. Sci.*, 2020, **13**, 3917–3949.
37 Q. Li, Y. B. Wang, F. N. Mo, D. H. Wang, G. J. Liang, Y. W. Zhao, Q. Yang, Z. D. Huang and C. Y. Zhi, *Adv. Energy Mater.*, 2021, **11**, 2003931.
38 N. Zhang, F. Y. Cheng, Y. C. Liu, Q. Zhao, K. X. Lei, C. C. Chen, X. S. Liu and J. Chen, *J. Am. Chem. Soc.*, 2016, **138**, 12894–12901.
39 W. Sun, F. Wang, S. Hou, C. Yang, X. Fan, Z. Ma, T. Gao, F. Han, R. Hu, M. Zhu and C. Wang, *J. Am. Chem. Soc.*, 2017, **139**, 9775–9778.
40 Y. Huang, J. Mou, W. Liu, X. Wang, L. Dong, F. Kang and C. Xu, *Nano-Micro Lett.*, 2019, **11**, 49.
41 L. T. Ma, Q. Li, Y. R. Ying, F. X. Ma, S. M. Chen, Y. Y. Li, H. T. Huang and C. Y. Zhi, *Adv. Mater.*, 2021, **33**, 2007406.
42 Y. Yang, C. Y. Liu, Z. H. Lv, H. Yang, Y. F. Zhang, M. H. Ye, L. B. Chen, J. B. Zhao and C. C. Li, *Adv. Mater.*, 2021, **33**, 2007388.
43 H. L. Pan, Y. Y. Shao, P. F. Yan, Y. W. Cheng, K. S. Han, Z. M. Nie, C. M. Wang, J. H. Yang, X. L. Li, P. Bhattacharya, K. T. Mueller and J. Liu, *Nat. Mater.*, 2016, **1**, 16039.
44 M. Fojtik, D. Kim, G. Chen, Y.-S. Lin, D. Fick, J. Park, M. Seok, M.-T. Chen, Z. Foo, D. Blaauw and D. Sylvester, *IEEE J. Solid-State Circuits*, 2013, **48**, 801–813.
45 J. H. Pikul, H. Gang Zhang, J. Cho, P. V. Braun and W. P. King, *Nat. Commun.*, 2013, **4**, 1732.
46 K. Sun, T. S. Wei, B. Y. Ahn, J. Y. Seo, S. J. Dillon and J. A. Lewis, *Adv. Mater.*, 2013, **25**, 4539–4543.
47 F. Le Cras, B. Pecquenard, V. Dubois, V. P. Phan and D. Guy-Bouyssou, *Adv. Energy Mater.*, 2015, **5**, 1501061.
48 H. M. Tang, D. D. Karnaushenko, V. Neu, F. Gabler, S. T. Wang, L. X. Liu, Y. Li, J. W. Wang, M. S. Zhu and O. G. Schmidt, *Small*, 2020, **16**, 2002410.
49 M. Sternad, G. Hirtler, M. Sorger, D. Knez, K. Karlovsky, M. Förster and H. M. R. Wilkening, *Adv. Mater. Technol.*, 2021, **7**, 2100405.
50 Q. Weng, S. Wang, L. Liu, X. Lu, M. Zhu, Y. Li, F. Gabler and O. G. Schmidt, *Cell Rep.*, 2021, **2**, 100429.
51 H. L. Ning, J. H. Pikul, R. Y. Zhang, X. J. Li, S. Xu, J. J. Wang, J. A. Rogers, W. P. King and P. V. Braun, *Proc. Natl. Acad. Sci. U. S. A.*, 2015, **112**, 6573–6578.

